Li, X. and Gao, Z. (2024) Evaluation of three weight functions for nonlocal regularisation of sand models. *International Journal of Geomechanics*, 24(7), 04024125. (doi: 10.1061/IJGNAI.GMENG-9192)

This is the author accepted version of the article. There may be differences between this version and the published version. You are advised to consult the published version if you wish to cite from it Please cite from the publisher version:
https://doi-org.ezproxy2.lib.gla.ac.uk/10.1061/IJGNAI.GMENG-9192

https://eprints.gla.ac.uk/316690/

Deposited on: 15 January 2024

Enlighten – Research publications by members of the University of Glasgow
http://eprints.gla.ac.uk

Evaluation of three weight functions for nonlocal regularisation of sand models

Xin Li[1] and Zhiwei Gao[2]

[1]Ph.D. Candidate, James Watt School of Engineering, University of Glasgow, Glasgow G12 8QQ, UK. Email: 2474559L@glasgow.ac.uk

[2]Senior Lecturer, James Watt School of Engineering, University of Glasgow, Glasgow G12 8QQ, UK (corresponding author). ORCID: https://orcid.org/0000-0002-5501-9855. Email: zhiwei.gao@glasgow.ac.uk

Abstract: Nonlocal regularisation is frequently used to resolve the mesh-dependency issue caused by strain softening in finite element (FE) simulations. Some or all the variables affecting strain softening are assumed to depend on the local and/or neighbouring ones in this method. The weight function is the most component of a regularisation method. There are three most widely used weight functions, including the Gaussian distribution (GD), Galavi and Schweiger (G&S) and over-nonlocal (ON) functions. Though all of them are found to alleviate or eliminate the mesh dependency in simple boundary value problems (BVPs) like plane strain compression, evaluation of their performance in real-world BVPs is rare. A detailed comparison of these functions has been carried out based on an anisotropic sand model accounting for the evolution of anisotropy. The increment of void ratio is assumed nonlocal. All functions give mesh-independent force-displacement relationship in drained and undrained plane strain compression tests. The shear band thickness shows a small variation when the mesh size is smaller than the internal length. None of them can eliminate the mesh dependency of shear band orientation. The G&S method is the most efficient in eliminating the mesh dependency in the strip footing problem. The ON method can give excessive overprediction of volume expansion around strip footings, leading to unrealistic low reaction forces on strip footings at large deformation. All three weight functions give mesh-independent results for the earth pressure acting on a retaining wall.

Keywords: Sand, constitutive model, strain softening, nonlocal regularisation, weight function

1. Introduction

The response of the FE continuum after it has reached its peak is inherently dependent on the mesh used, as noted by Bazant and Jirasek (2002). For strain localisation analysis, the FE solution will converge to a unique one as the mesh size gets smaller, when a strain-hardening model is used (e.g., Galavi and Schweiger, 2010; Lu, et al., 2019). But such convergence cannot be obtained when a strain-softening model is used (e.g., Mallikarachchi and Soga, 2020; Gao et al., 2022). Mathematically, this mesh dependency is linked to the transformation of the governing partial differential equations from elliptic to hyperbolic, which occurs when the material behaviour transitions from hardening to softening. Previous research has also highlighted this issue (e.g., Mühlhaus, 1986; Galavi and Schweiger, 2010; Guo and Stolle, 2013; Lu, et al., 2019; Cui et al., 2023). Alsaleh et al. (2006) have pointed out that the FE simulation of strain localization is subject to mesh dependency due to the use of classical continuum models that do not account for micro-structural factors, such as particle size and associated voids.

Different methods have been proposed to resolve the mesh-dependency issue, including the strain-gradient enhanced approaches (e.g., Aifantis, 1984; de Borst and Mühlhaus, 1992; Dorgan and Voyiadjis, 2003), micro-polar plasticity approach (e.g., Mühlhaus, 1986; Alshibli et al., 2006; Tang et al., 2013), nonlocal regularisation method (e.g., Eringen, 1972; Lü et al., 2009; Galavi and Schweiger, 2010; Guo and Stolle, 2013; Lazari et al., 2015; Summersgill et al., 2017; Mallikarachchi and Soga, 2020; Singh et al., 2021; Gao et al., 2022; Cui et al., 2023) and viscous plasticity theory (e.g., Oka, et al., 1995; Wang, et al. 1997; Higo, 2004; Yin et al. 2010). An internal length scale is introduced to the constitutive model formulation in these methods, which controls the degree of deformation localisation and preserves the well-posedness of the governing partial differential equations irrespective of the refinement of the mesh (de Borst et al., 1993). Among these methods, nonlocal regularisation is the most widely used for advanced soil models. Nonlocal methods are proposed based on the hypothesis that the response of materials depends on the deformation field of a local material point and a weighted average of its neighbouring points (Mallikarachchi, 2019).

The weight function is the most important component of a nonlocal regularisation method. The GD function has been used in many early studies (Eringin, 1974; Bažant et al., 1984). The variable at the current stress point contributes most to the nonlocal one, and therefore, the nonlocal variable is concentrated at the local point and cannot spread to surrounding points. Galavi and Schweiger (2010) proposed a new weight function in which the local variable does not affect the nonlocal one. Moreover, Vermeer and Brinkgreve (1994) have proposed the over-nonlocal method which uses a linear combination of the local and the nonlocal variables. A nonlocal parameter m is introduced to control the proportion of local and nonlocal variables in weight functions. Some studies have been done on the comparison of these methods in simple BVPs like plane strain compression. It is found that the G&S gives better regularisation results than the GD one (Galavi and Schweiger, 2010; Guo and Stolle, 2013; Summersgill et al., 2017; Mallikarachchi and Soga, 2020; Gao et al., 2022). But the performance of these functions in real-world BVPs has not been evaluated.

The main aim of this study is to carry out a comprehensive comparison of these functions in various BVPs, including drained and undrained plane strain compression, the response of strip footings on level ground and near a slope and a retaining wall (passive and active conditions). An anisotropic sand model accounting for the evolution of anisotropy is used. The increment of the void ratio which has a significant influence on the strain softening is assumed nonlocal. The three nonlocal weight functions and constitutive model will be first introduced. The performance of the regularisation methods will then be compared in different BVPs.

2. The weight functions for nonlocal regularisation

The GD function was first introduced by Eringin (1974) and then successfully implemented in damage models with strain softening (Bažant et al., 1984). It is expressed as

$$\omega_i = \frac{1}{\sqrt{\pi} l_c} \exp\left(-\frac{r_i^2}{{l_c}^2}\right) \tag{1}$$

where ω_i represent the weight function of integration point i, r_i is the distance between the current integration point and the $i-th$ integration point, l_c is a nonlocal parameter termed internal length which is dependent on the mean size of soil particles (Galavi and Schweiger, 2010). Fig. 1 shows the physical significance of internal length in a 2D problem. Fig. 2 shows the plot of Eq. (1) in 1D condition. It is obvious that the GD function shows the highest contribution to the calculated nonlocal variable at the centre and diminishes along the distance. As mentioned by Vermeer and Brinkgreve (1994), the nonlocal variable is concentrated at the local point and cannot spread to surrounding points which has a negative effect on the nonlocal method. This results in a centre concentration of the softening variable when local strain is treated as a nonlocal variable.

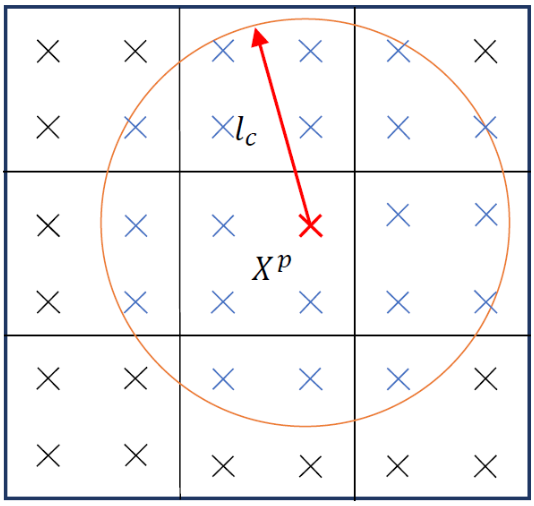

Fig. 1 Schematic diagram showing neighbouring integration point of X^{P}

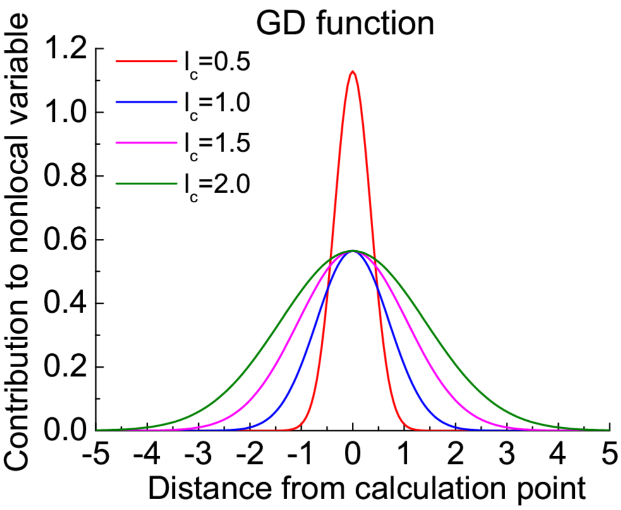

Fig. 2 The Gaussian distribution function in 1D condition

Based on the hypothesis that the deformation at a point is more influenced by the response at the neighbourhood rather than the concentrated deformation at the point itself, Galavi and Schweiger (2010) have proposed the following weight function

$$\omega_i = \frac{r_i}{{l_c}^2} \exp\left(-\frac{r_i^2}{{l_c}^2}\right) \tag{2}$$

As shown in Fig. 3, the contribution of the G&S weight function to the calculated nonlocal variable is zero in the centre point and efficiently spreads from the concentrated local point to a larger zone. This is different from the GD function with the maximum value at the centre. In addition, the G&S weight function shows two same peaks with a distance of $0.707l_c$ from the centre (Galavi and Schweiger, 2010).

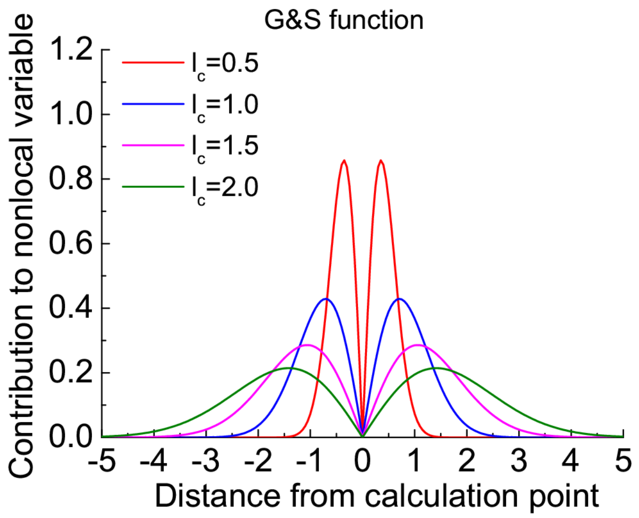

Fig. 3 The Galavi and Schweiger (2010) distribution function in 1D condition

Moreover, another method to overcome the limitations of Gaussian distribution is proposed by Vermeer and Brinkgreve (1994), which is a linear combination of the local and the nonlocal variables. A nonlocal parameter m is applied to change the nonlocal averaging formulation. This method was called the over-nonlocal method. The nonlocal variable is expressed as

$$\bar{\varpi}(x) = (1-m)\varpi(x) + \frac{m}{V}\int_V \omega(x,\xi)\,\varpi(\xi)d\xi \tag{3}$$

where $\bar{\varpi}(x)$is the nonlocal variable and $\varpi(x)$ is the local variable. The parameter m provides the relative contribution from local and nonlocal parts. When $m\ < 1$ in Eq. (3), the nonlocal variable produces less effect than the local one. On the contrary, the contribution of the local variable will be negative when $m > 1$. Existing research has shown that $m > 1$ should be used to achieve the best regularisation results (Vermeer & Brinkgreve, 1994; Lü et al., 2009; Xue et al., 2022). But the exact value is dependent on the model and has to be determined via trial and error.

3 The constitutive model and nonlocal regularisation

3.1 Constitutive model

The constitutive model used here has been presented by Gao et al. (2022). Only the yield function and plastic hardening law which affect the strain softening are given here. The yield function is expressed as

$$f = \frac{R}{g(\theta)} - H = 0 \tag{4}$$

where $R = \sqrt{\frac{3}{2} r_{ij} r_{ij}}$, with $r_{ij} = (\sigma_{ij} - p\delta_{ij})/p$, σ_{ij} is the stress tensor, $p = \sigma_{ii}/3$ is the mean effective stress, δ_{ij} is the Kronecker delta ($= 1$ for $i = j$, and $= 0$ for $i \neq j$), H is the hardening parameter and $g(\theta)$ is an interpolation function which describes the variation of critical state stress ratio with the Lode angle θ of r_{ij} (Li and Dafalias, 2002).

The hardening law for the yield function (evolution of for H) is expressed as

$$dH = \langle L \rangle r_H = \langle L \rangle \frac{G h_1 e^{h_2 A}}{(1+e)^2 \sqrt{p p_a} R} [M_c g(\theta) e^{-n\zeta} - R] \tag{5}$$

where h_1, h_2, and n are three model parameters; A is the anisotropic variable (Li and Dafalias, 2012); G is the elastic shear modulus; L is the loading index and $\langle \quad \rangle$ are the Macaulay brackets which make $\langle L \rangle = L$ for $L > 0$ and $\langle L \rangle = 0$ for $L \leq 0$; p_a is the atmospheric pressure (101 kPa); M_c is the critical state stress ration in triaxial compression; e is the void ratio, and ζ is the dilatancy state parameter. The expression of $g(\theta)$ can be found in Gao et al. (2022).

It is evident that several variables affect plastic hardening, and thus, strain softening (Gao et al., 2022). But only the increment of void ratio is assumed nonlocal for two main reasons (Gao et al., 2022). First, the void ratio is a key state variable that affects the behaviour of sand. Secondly, making the other state variables nonlocal can be computationally expensive. The increment of the nonlocal void ratio is expressed below

$$de = (1 + e) d\varepsilon_{vn} \tag{6}$$

$$d\varepsilon_{vn} = \frac{\sum_{k=1}^{N} w_i v_i d\varepsilon_{vi}}{\sum_{k=1}^{N} w_i v_i} \tag{7}$$

where positive de means volume contraction and $d\varepsilon_{vn}$ is the nonlocal volumetric strain increment, N is the number of integration points within the averaging area, v_i and $d\varepsilon_{vi}$

represent the volume and local volumetric strain increment of integration point i. Eq. (6) and (7) can be used for the GD and G&S functions. When the over-nonlocal method is used, the void ratio increment is expressed as

$$de = (1+e)[(1-m)d\varepsilon_{vl} + md\varepsilon_{vn}] \tag{8}$$

where $d\varepsilon_{vl}$ is the total local volumetric strain increment for each step. In Eq. (8), $d\varepsilon_{vn}$ is calculated using the GD function.

3.2 Implementation of the nonlocal method

The model used the explicit stress integration method (Zhao et al., 2005; Gao and Zhao, 2013; Zhou, et al., 2021; Zhou, et al., 2022; Lu, et al. 2023) and two user subroutines, UMAT (user-defined materials) and USDFLD (user-defined field variables), are needed for implementing the nonlocal method in Abaqus.

To increase the computation efficiency, a scaling variable r_v defined as below is introduced (Gao et al., 2021)

$$r_v = \frac{d\varepsilon_{vn}}{d\varepsilon_{vl}} \tag{9}$$

where $d\varepsilon_{vn}$ is the nonlocal volumetric strain increment and $d\varepsilon_{vl}$ is the total local volumetric strain increment for each increment. Both of them are calculated before the sub-increment of strain is applied in the stress integration.

At the end of each sub-increment the void ratio increment de^s is

$$de^s = (1+e)d\varepsilon_{vl}^s r_v \tag{10}$$

where $d\varepsilon_{vl}^s$ is the local sub-increment of volumetric strain (Gao et al., 2022). The summation of de^s at all sub-increments is the total void ratio change in a step. For the over-nonlocal method, de^s is calculated below

$$de^s = (1+e)[(1-m)d\varepsilon_{vl}^s + md\varepsilon_{vl}^s r_v] \tag{11}$$

4. Plane strain compression tests

The sample used in this study is 60 mm wide and 120 mm high as shown in Fig. 4. The boundary condition is shown in Fig. 4. A confining pressure of $p_0 = 200$kPa is applied on the two vertical sides. Vertical displacement is applied on the top side with the horizontal displacement unconstrained. The bottom side is pinned at the left and free to move to the right. A square 'weak' area (12mm×12mm) with inclined bedding plane orientation ($\alpha = 45°$) is implemented, which is used to trigger a shear band in the plane strain compression test. For the remaining part of this specimen, the bedding plane orientation is horizontal and $\alpha = 0°$. The anisotropic model parameters are shown in Table 1. All the parameters are the same as those in Gao et al. (2022). Note that the parameter m_d is m in Gao et al. (2022). The initial void ratio of the sample is $e_0 = 0.65$ (relative density $D_r = 85.6\%$), and the initial degree of anisotropy is $F_0 = 0.4$. All simulations in this study have used 8-noded plane strain quadratic elements with reduced integration (CPE8R). Note that all the simulations to be presented below use this element. The thickness of the soil is assumed 1m in processing the results.

The internal length l_c is an important parameter for nonlocal regularisation models. The size of the internal length determines how many integration points can be involved in nonlocal regularisation. l_c should be equal to or larger than the maximum mesh size to make sure that sufficient integration points are involved. Bigger l_c means that the stress and strain relationship of the current integration point is affected by that of integration points further away. Fig. 5 illustrates the effect of l_c on the vertical reaction force and displacement curves simulated by the different weight functions. In these models, the mesh size of 0.004 m was selected under drained conditions. The l_c is does not affect the solutions before the peak reaction force. Higher peak vertical reaction force and a slower rate of strain-softening were obtained by increasing l_c during post-peak. Furthermore, the GD and ON functions predict a slower rate of the strain-softening curve than the GD function. The internal length determines the range within which the integration points are considered in the nonlocal averaging. When it is bigger, more integration points are accounted for in the weight functions of each integration point. This means that the local load is artificially distributed to more neighbouring integration points, leading to a lower rate of strain softening . In the simulations for plane strain compression below, $l_c = 0.012\,m$ is used. It should be mentioned that l_c also has influence on the shear band thickness, which will be shown in subsequent sections. The real shear band thickness of sand is about 10-20d_{50}, where d_{50} is mean particle size (Galavi and Schweiger, 2010). If the real shear band thickness were to be matched in FE modelling, very small mesh size has to be used because the shear band thickness is close to l_c. This would cause issues like excessive computation time and numerical divergence. Therefore, proper l_c

is typically chosen based on the size of solution domain, which can guarantee mesh-independent results but not realistic shear band thickness.

Table 1 Model parameters for Toyoura sand

Parameters	Value
G_0	125
ν	0.1
M_c	1.25
c	0.75
e_Γ	0.934
λ_c	0.019
ξ	0.7
n	2.0
h_1	0.45
d_1	1.0
m	3.5
k_f	0.5
e_A	0.075
k_h	0.03
h_2	0.5

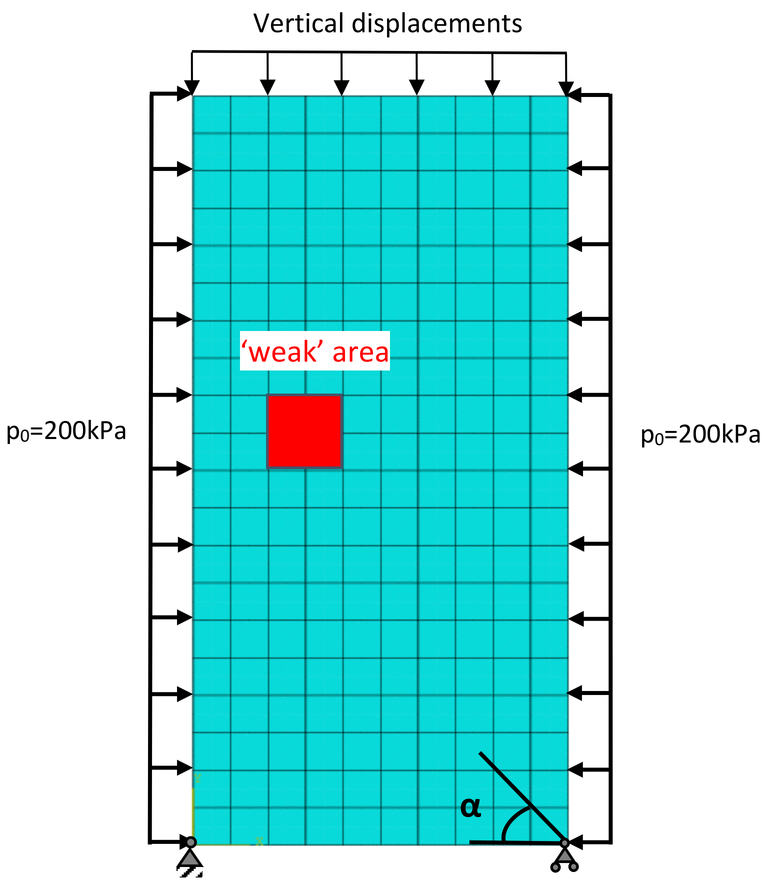

Fig. 4 The boundary conditions and bedding plan orientation for the plane strain compression simulations

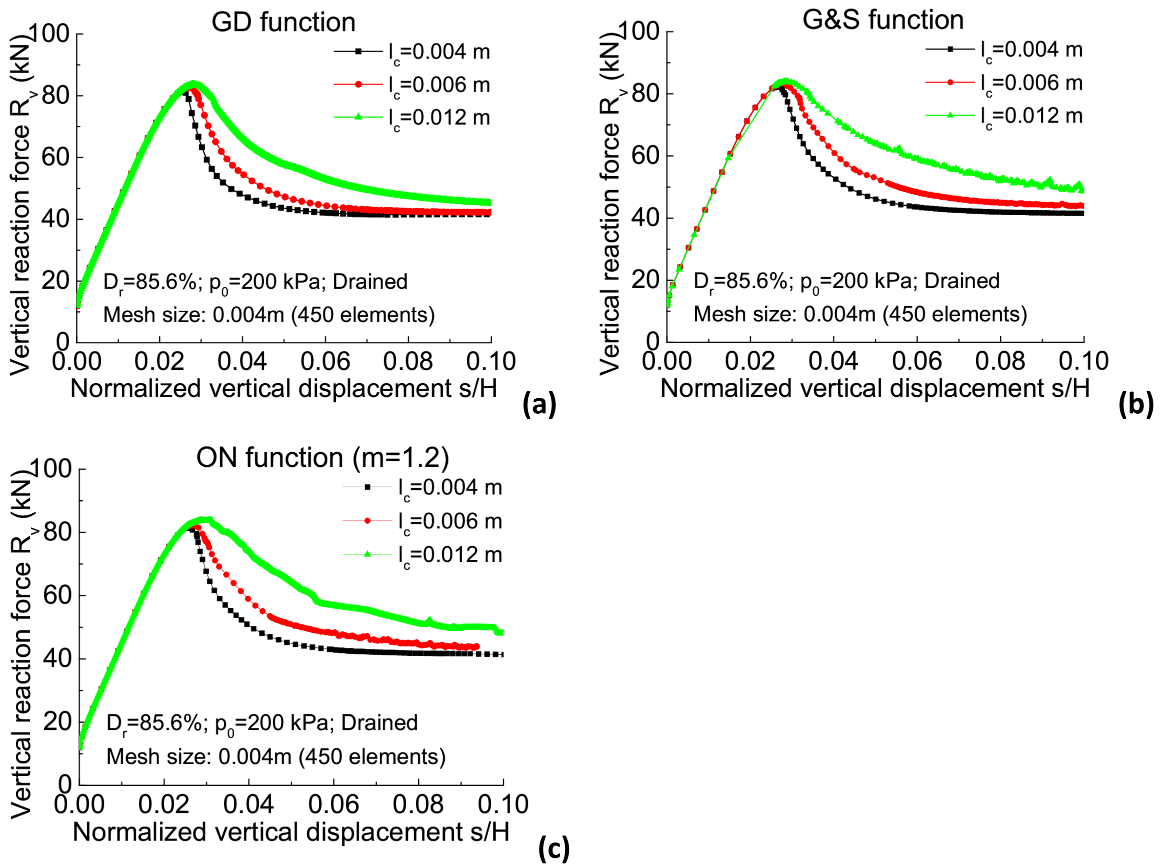

Fig. 5 The effect of internal length on the force-displacement relationship in drained plane strain compression test: (a) GD function; (b) G&S function; (c) ON function

4.1 Drained plane strain compression tests

Fig. 6 shows the force-displacement curves predicted by the local model and three nonlocal models. The GS and ON functions give better regularisation results than the GD one. The main reason is that the local variable has more significant influence on the results when the GD function is used. It should be mentioned that $m = 1.2$ is chose for the ON method through trial-and-error. Smaller m gives mesh-dependent solutions, but higher m causes numerical divergence in the simulations. In the strip footing problem to be discussed in the subsequent sections, higher m is found to give steep reduction of reaction force acting on the footing after peak, which is not consistent with the experimental observations in centrifuge tests.

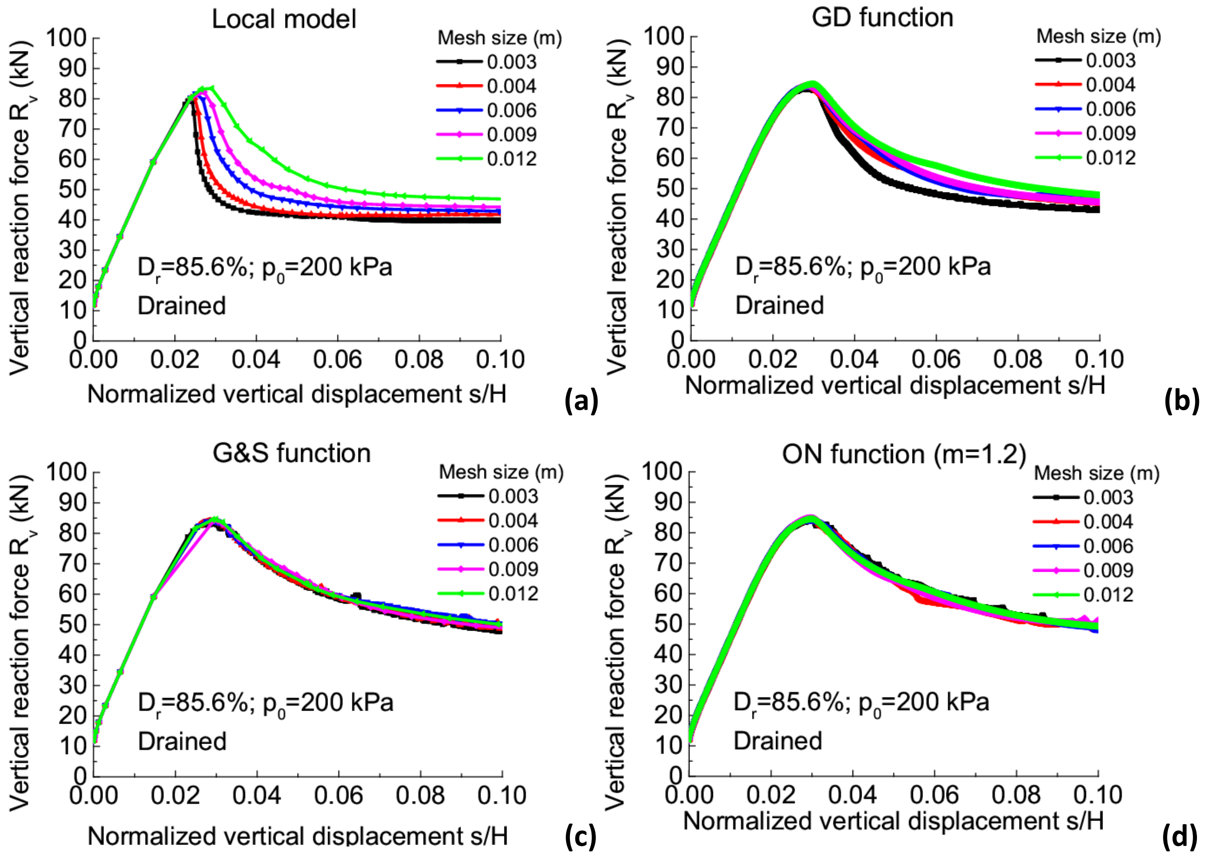

Fig. 6 Comparison of the local and nonlocal models on the force-displacement relationship for drained plane strain compression: (a) Local model; (b) GD function; (c) G&S function; (d) ON function

The orientation of the shear band (β) is directly measured from shear strain contours as shown in Fig. 7. The predicted angle of shear band orientation decreases as the mesh size increases (Fig. 8). All the nonlocal functions reduce but cannot eliminate the mesh dependency of shear band orientation. This could be due to that only one variable that affects the strain softening is assumed nonlocal. The mesh dependency could be further reduced if more state variables in the hardening law are assumed nonlocal. But this would significantly reduce the computation efficiency.

The thickness of shear band is measured based on the shear strain distribution across a shear band at $s/H = 7\%$ (Fig. 9). Fig. 10 shows the determination of shear band thickness for the nonlocal model. In Fig. 10 (a) t_{s1} and t_{s2} represent shear band thickness for mesh size 0.004 m and 0.006 m, respectively. The effect of mesh size on shear band thickness is shown in Fig. 11 (a). The shear band thickness simulated by the local model increases significantly with the mesh size. The nonlocal models give a small variation of shear band thickness when the mesh size $h < l_c$. All nonlocal models give the same shear band thickness as that of the local model when size $h = l_c$. The shear band thickness predicted by the nonlocal models increases with l_c (Fig. 11b) and the ON model predicts wider shear bands.

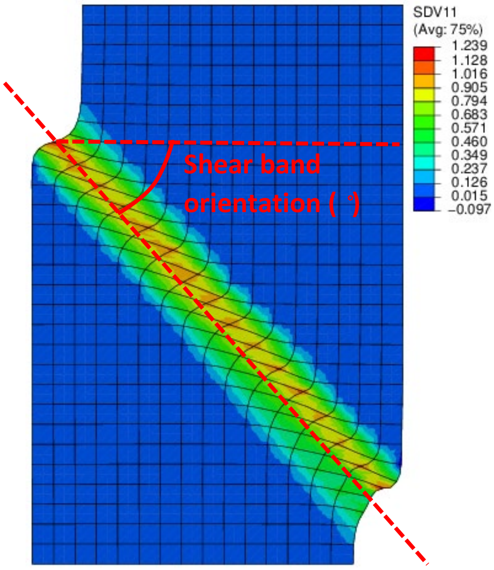

Fig. 7 Shear strain contour for measuring the shear band orientation

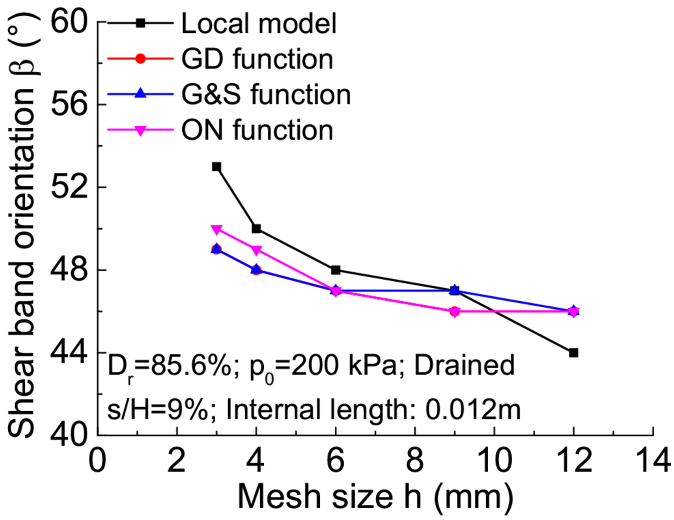

Fig. 8 Comparison of shear band orientation for drained plane strain compression test

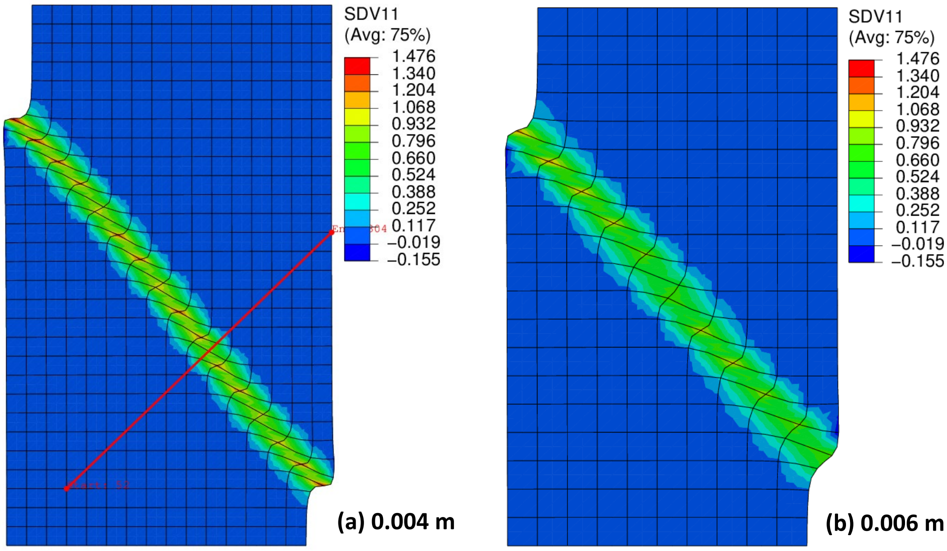

Fig. 9 Cross-section contour based on the shear strain under drained condition with mesh size of (a) 0.004 m and (b) 0.006 m for the local model

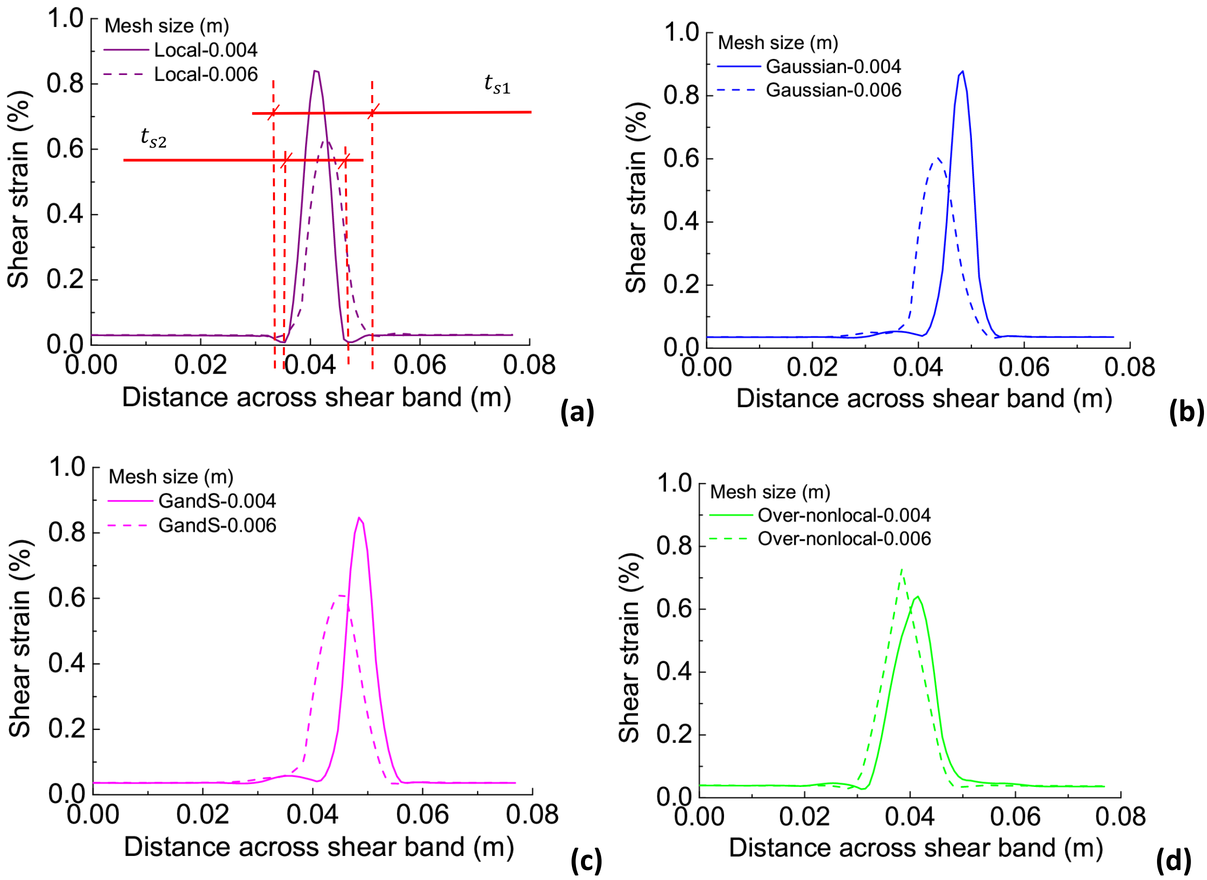

Fig. 10 Comparison of cross-section profiles based on the shear strain: (a) Local model; (b) GD function; (c) G&S function; (d) ON function

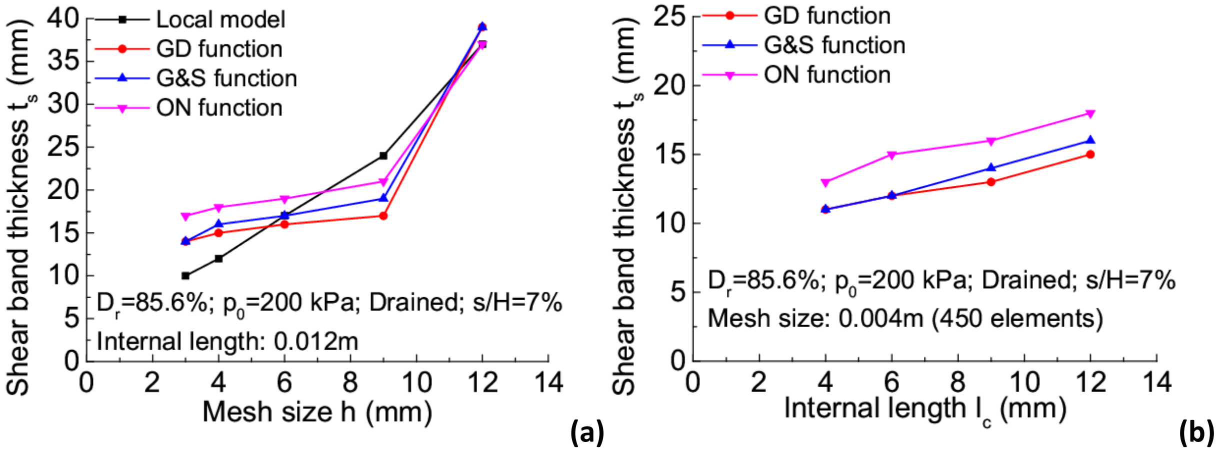

Fig. 11 Comparison of the effect of (a) mesh size and (b) internal length on the shear band thickness in plane strain compression

4.2 Undrained plane strain compression tests

In undrained plane strain compression, the permeability of soil is set very small and water flow at all boundaries is closed. Fig. 12 shows the relationship between vertical displacement and reaction force for different models. It is evident that the nonlocal models give mesh-independent results.

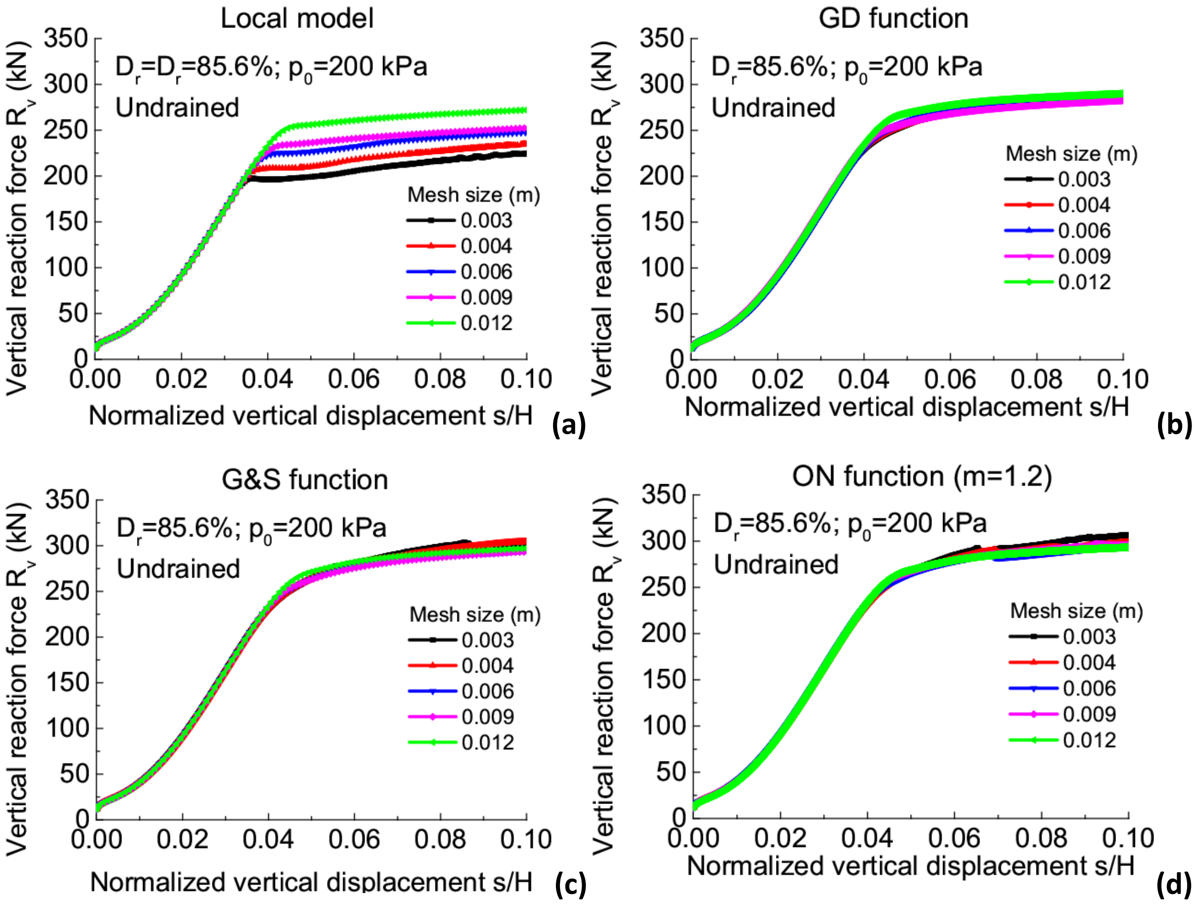

Fig. 12 Comparison of the force-displacement relationship for undrained plane strain compression test: (a) Local model; (b) GD function; (c) G&S function; (d) ON function

The shear band orientation in undrained plane strain compression increases when the mesh is refined for all models. The mesh dependency can be reduced but not eliminated by the nonlocal treatment (Fig. 13). It is worth noting that the nonlocal models give the same shear band orientation as the local model when the mesh size is greater than 0.009 m. The nonlocal models also give a bigger variation of shear band orientation in undrained tests than in drained tests. The main reason is that there is a smaller change in the void ratio in an undrained test, which makes the nonlocal regularisation using the void ratio less effective. The shear band thickness predicted by the models is shown in Fig. 14. Similar to the drained cases, the nonlocal models give a small variation of shear band thickness when the mesh size is smaller than the internal length. But the shear band thickness predicted by the nonlocal models at $h = l_c$ is bigger than that of the local model. Moreover, it is found that the drainage condition has little influence on the shear band thickness at different internal lengths (Fig. 14b).

Fig. 15 shows the force and displacement relationship for loose sand in undrained plane strain compression. Though the vertical reaction force decreases after the peak, the mesh size has little influence on the results when the original model is used (Fig. 15a). The nonlocal models give similar results (Fig. 15c-d). The reason is that the stress ratio of soil elements keeps increasing though the deviator stress decreases. This is a strain-hardening response based on the model, as increasing stress ratio means increasing hardening parameter H (Eq. 5). In coupled dynamic loading (e.g., earthquake), the soil response will be a combination of that in Fig. 12 and Fig. 15, wherein the nonlocal regularisation method is found to work. Therefore, it is expected that the nonlocal regularisation technique also works for coupled analysis in earthquakes.

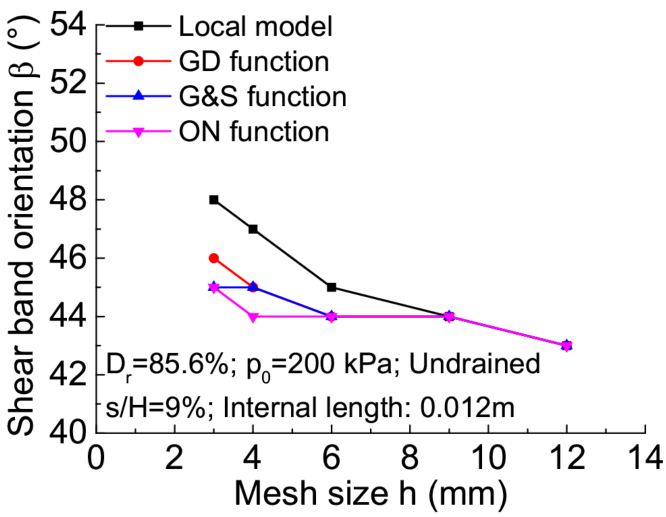

Fig. 13 Shear band orientation predicted by different models in undrained plane strain

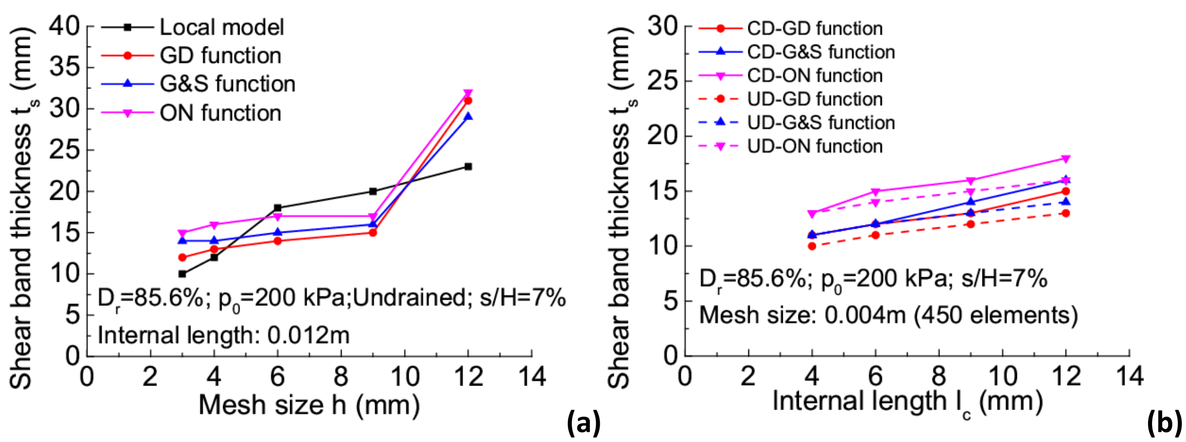

Fig. 14 Comparison of the effect of (a) mesh size and (b) internal length on the shear band thickness under undrained condition

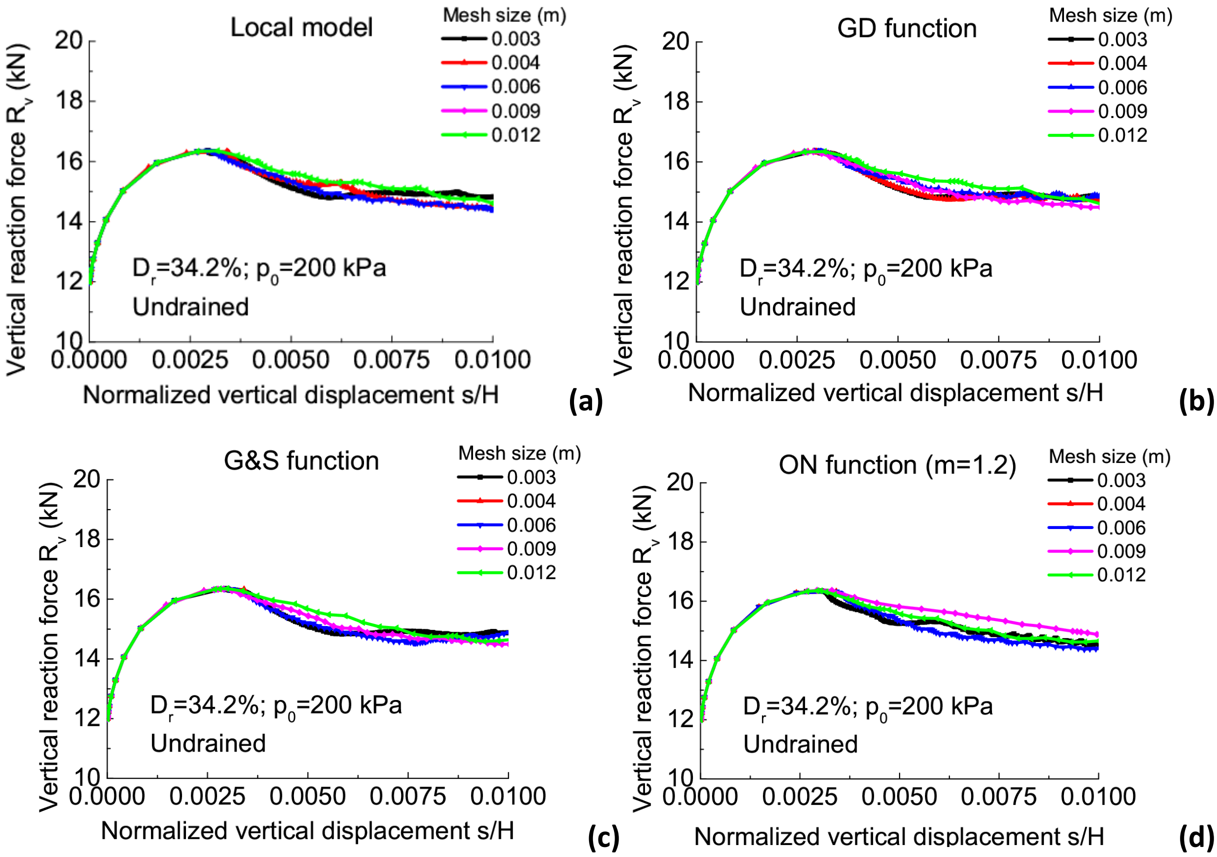

Fig. 15 Comparison of the force-displacement relationship for static limited liquefaction test: (a) Local model; (b) GD function; (c) G&S function; (d) ON function

5. Strip footing problem

5.1 Strip footing on level sand ground

The dimension of the strip footing problem is shown in Fig. 16. The footing with B=0.9 m is deformed by applying a uniform vertical deformation. The horizontal displacement is fixed to simulate rough footings. Constant vertical pressure (1 kPa) is applied on the top surface to avoid soil collapse with zero mean effective stress. The initial lateral earth pressure coefficient $K_0 = 0.4$ (Okochi and Tatsuoka 1984), and the effective weight of Toyoura sand is $\gamma' = 16\mathrm{kN/m^3}$ as there is no water in the sand. Two sides of the sample are horizontally fixed, while both horizontal and vertical movement is restricted for the bottom boundary. Details can be found in Gao et al. (2020). Since the vertical load and vertical settlement relationship is mainly affected by the rectangle area beneath the footing, hence, the mesh size far away from the footing is setting a fixed value (0.6m) for all models. The bedding plane orientation is horizontal and $\alpha = 0^{\circ}$. The relative density $D_r = 85.6\%$ and the initial degree of anisotropy is $F_0 = 0.4$.

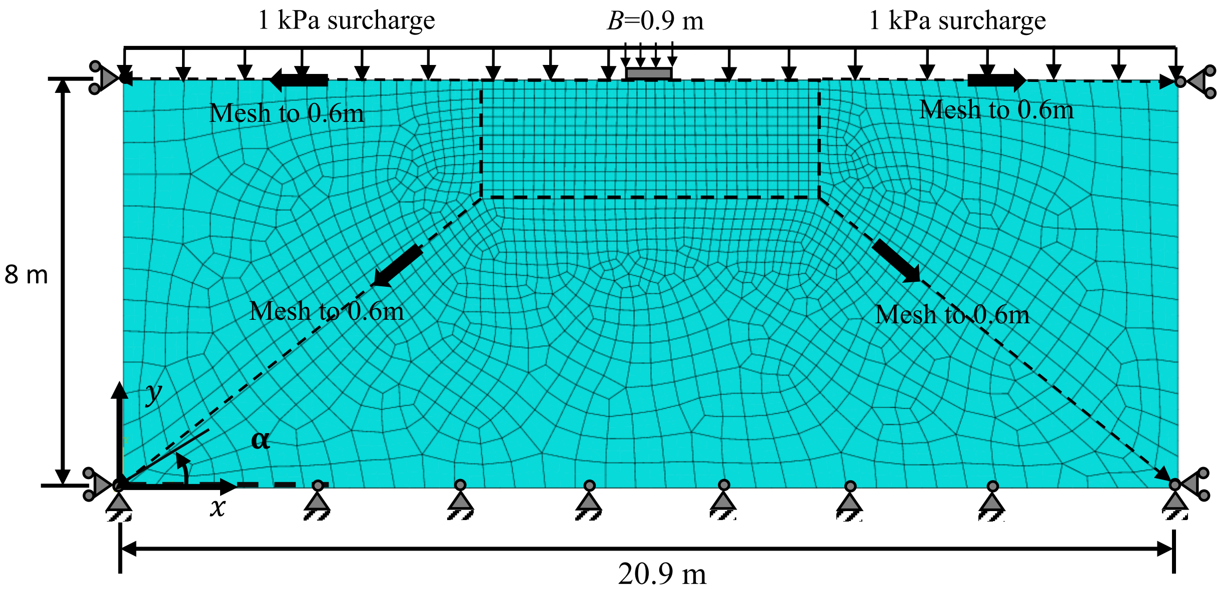

Fig. 16 The boundary conditions of strip footing problem

Fig. 17 shows the prediction of local and nonlocal models with $l_c = 0.8\ m$. It is evident that the local model prediction is highly mesh dependent. The G&S function gives the least mesh-dependent results. The strain softening predicted by the GD and G&S functions are in good agreement with the centrifuge test data (Kimura et al., 1985). But the ON model give very steep reduction of Q after the peak, which does not match the experimental observations. There are two reasons for this. First, this method gives excessive volume expansion of sand under the strip footing (Fig. 18). Location of the elements in Fig. 18 is shown in Fig. 19. The GD and GS models give similar prediction of void ratio evolution, while the void ratio increase predicted by the ON model is about 90% higher. Higher void ratio causes lower strength and failure of some elements, which lead to fast reduction of Q. Secondly, the ON method assumes that the local variable makes negative contribution to the local one, which may not be realistic. In this cases, such assumption causes failure or lower shear strength of more sand elements. Moreover, it is found that bigger m value gives even steeper strain softening curve for the ON function. Therefore, the ON function should not be used for this problem.

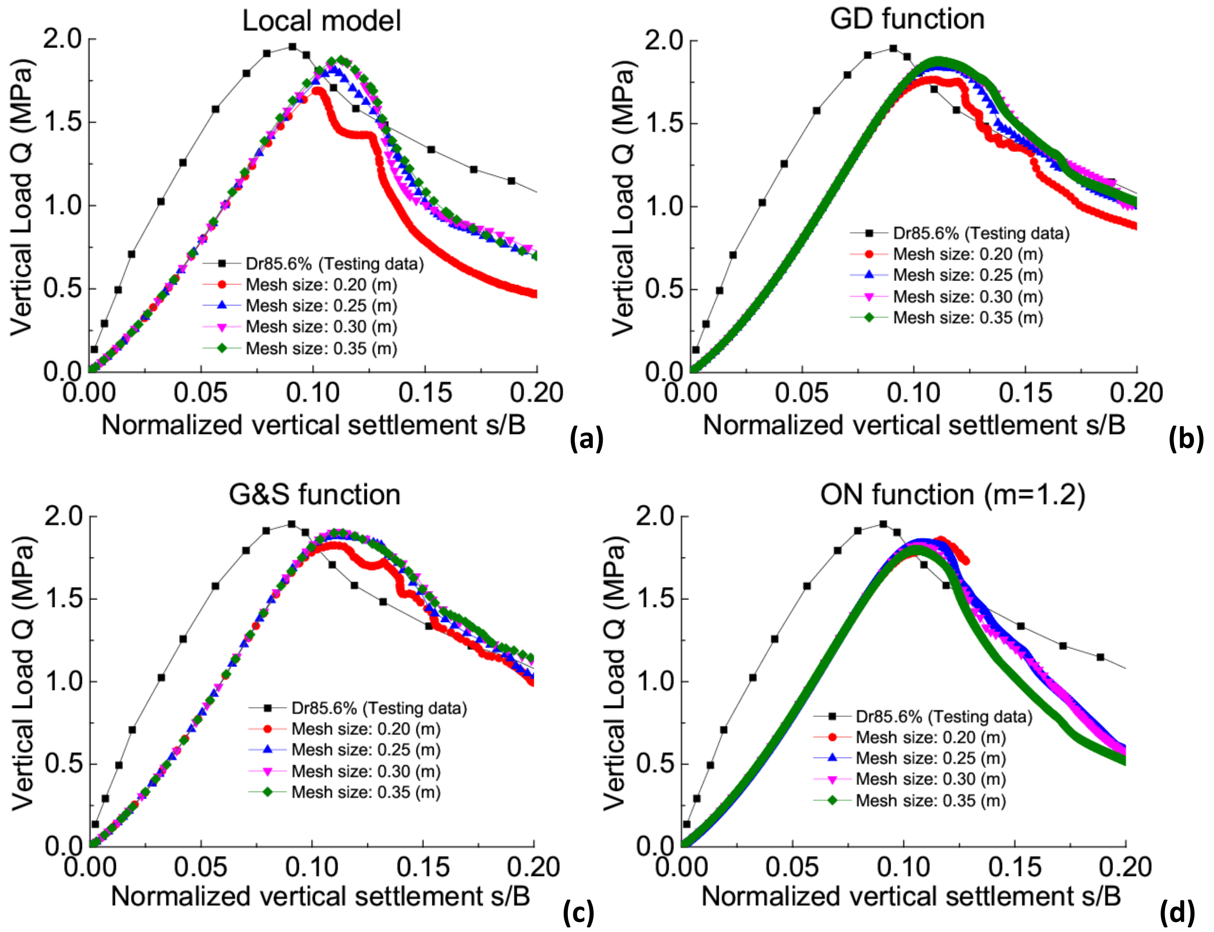

Fig. 17 The comparison of the strip footing response on the sand with horizontal bedding plane: (a)Local model; (b) GD function; (c) G&S function; and (d) ON function

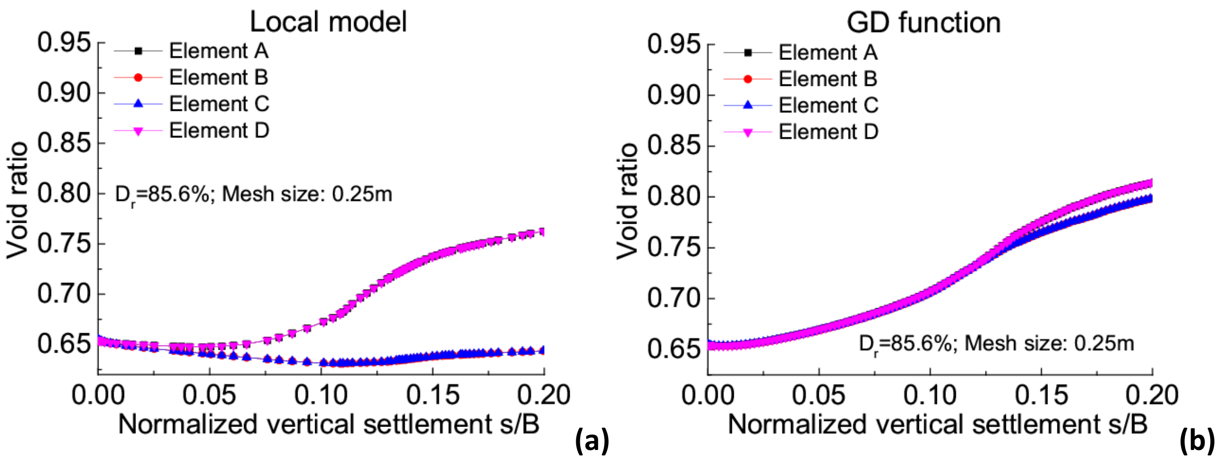

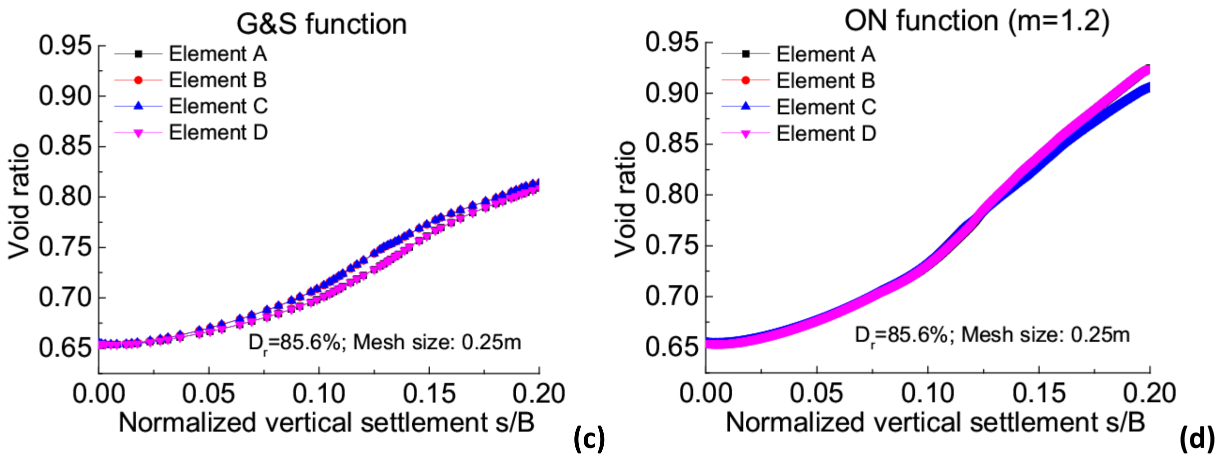

Fig. 18 Comparison of void ratio evolution for elements under the strip footing: (a) Local model; (b) GD function; (c) G&S function; (d) ON function

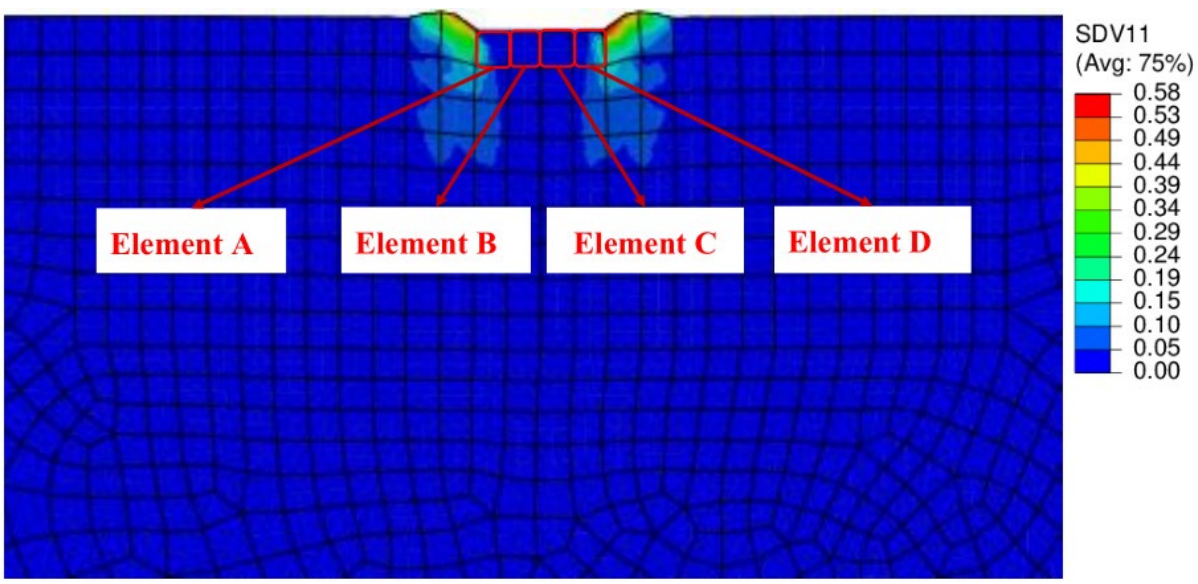

Fig. 19 Location of elements under the strip footing

5.2 Strip footing near a sand slope

This problem is based on the simulations in Gao et al. (2021). The slope dimension and boundary conditions are shown in Fig. 20. Since the ground surface is not level, a constant K_0 cannot be applied. Therefore, the gravity loading method is used to generate the initial stress state (Gao et al., 2021). First, gravity is applied on the same soil body by assuming that the soil is elastic with a Poisson's ratio of $\nu = 0.286$, making $K_0 = 0.4$ for a flat groud surface (Gao et al., 2021). After that, the stress state is extracted and imported to the model as the initial stress, which is used for the subsequent modelling. The soil density, initial void ratio and degree of anisotropy are the same as those in Fig. 16.

Fig. 21 shows the prediction of local and nonlocal models with $l_c = 0.4\ m$. The local model gives different peak bearing capacity and $s - Q$ curves after the peak as the mesh size changes (Fig. 21a). Nonlocal regularization reduces the mesh-dependent of $s - Q$ curves (Fig. 21c-d). The rate of strain softening is also reduced due to the nonlocal averaging of void ratio increment. To further reduce the mesh sensitivity, more nonlocal variables could be used, but this may increase the complexity of the model formulations and its implementation. Fig. 22 shows the contour of shear strain distribution in the soil after the state for G&S function. A clear slip surface can be seen, which is independent of the mesh size.

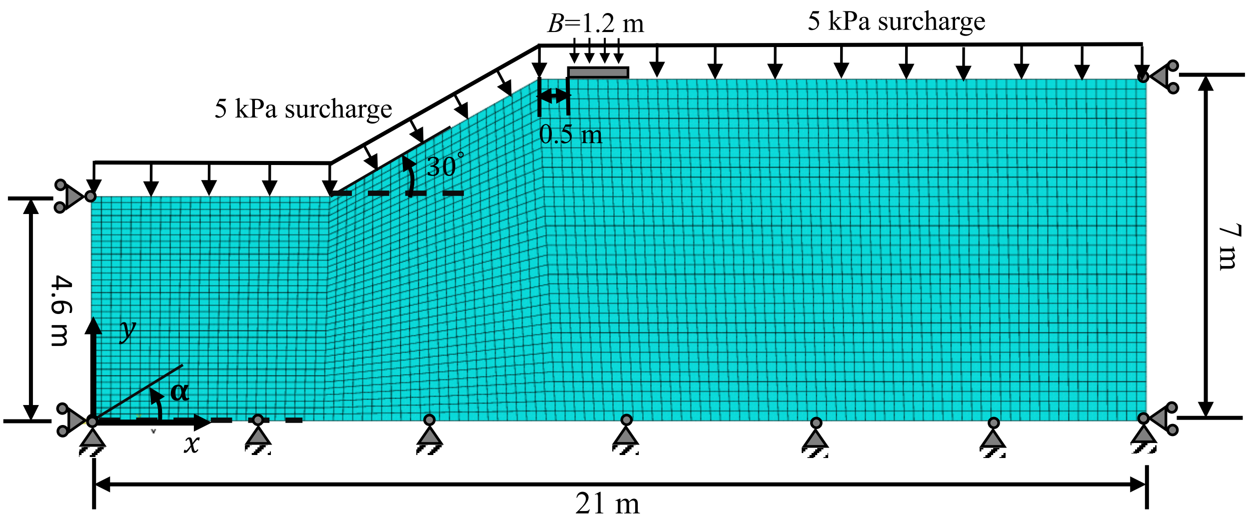

Fig. 20 The boundary conditions of the strip footing near a slope

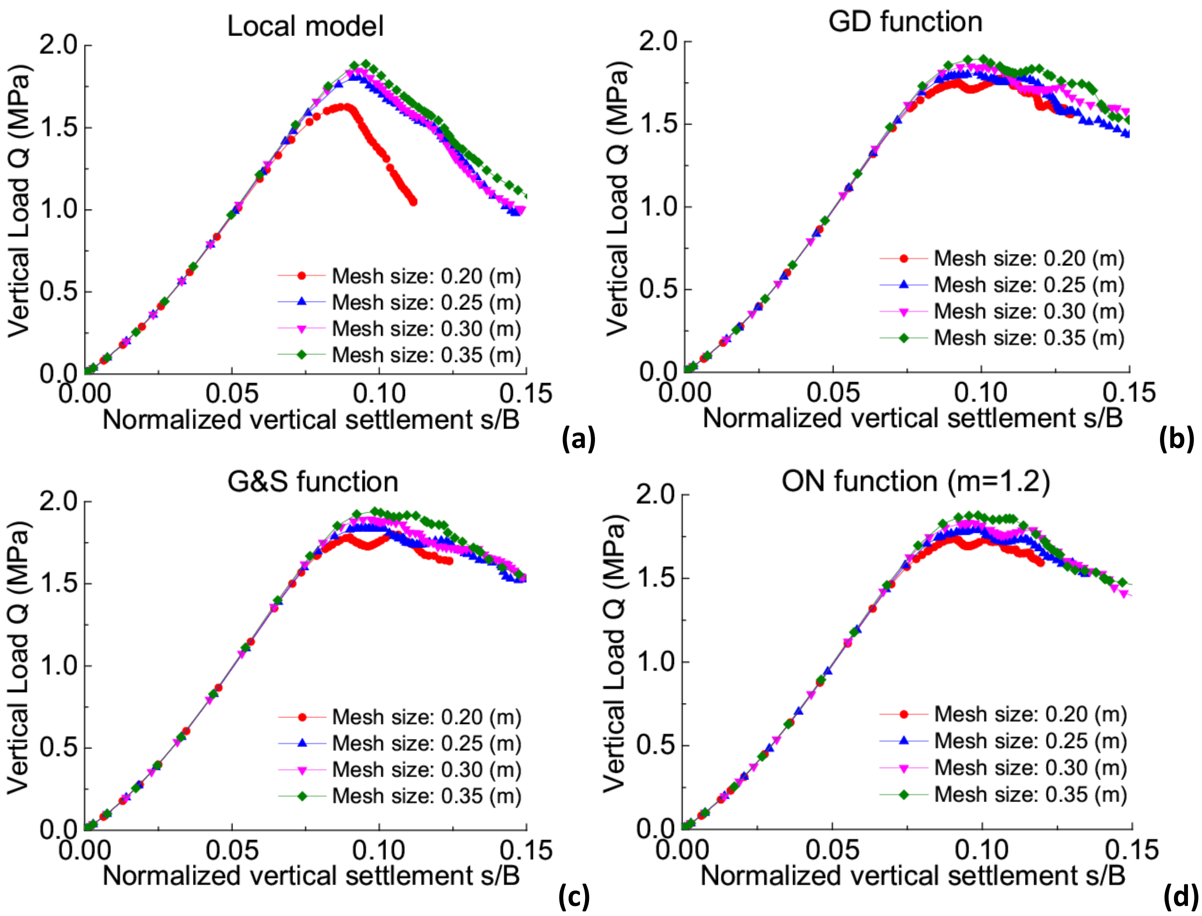

Fig. 21 The comparison of the strip footing response near a slope with horizontal bedding plane: (a) Local model; (b) GD function; (c) G&S function; (d) ON function

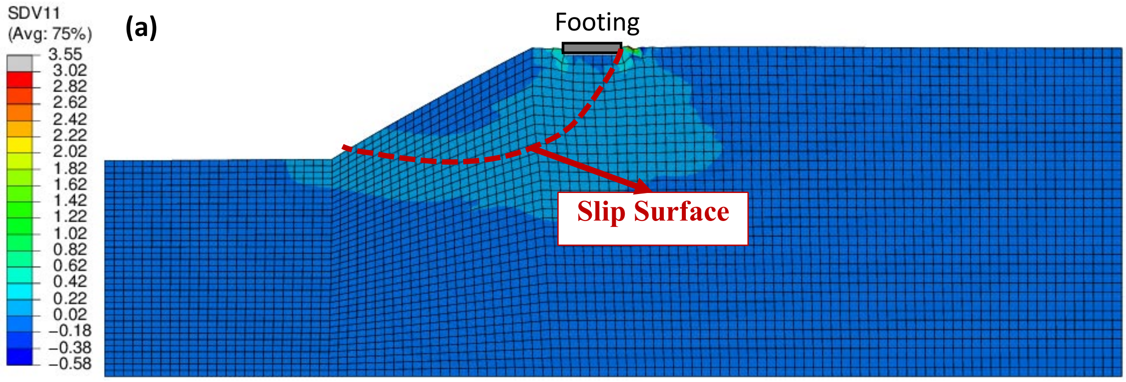

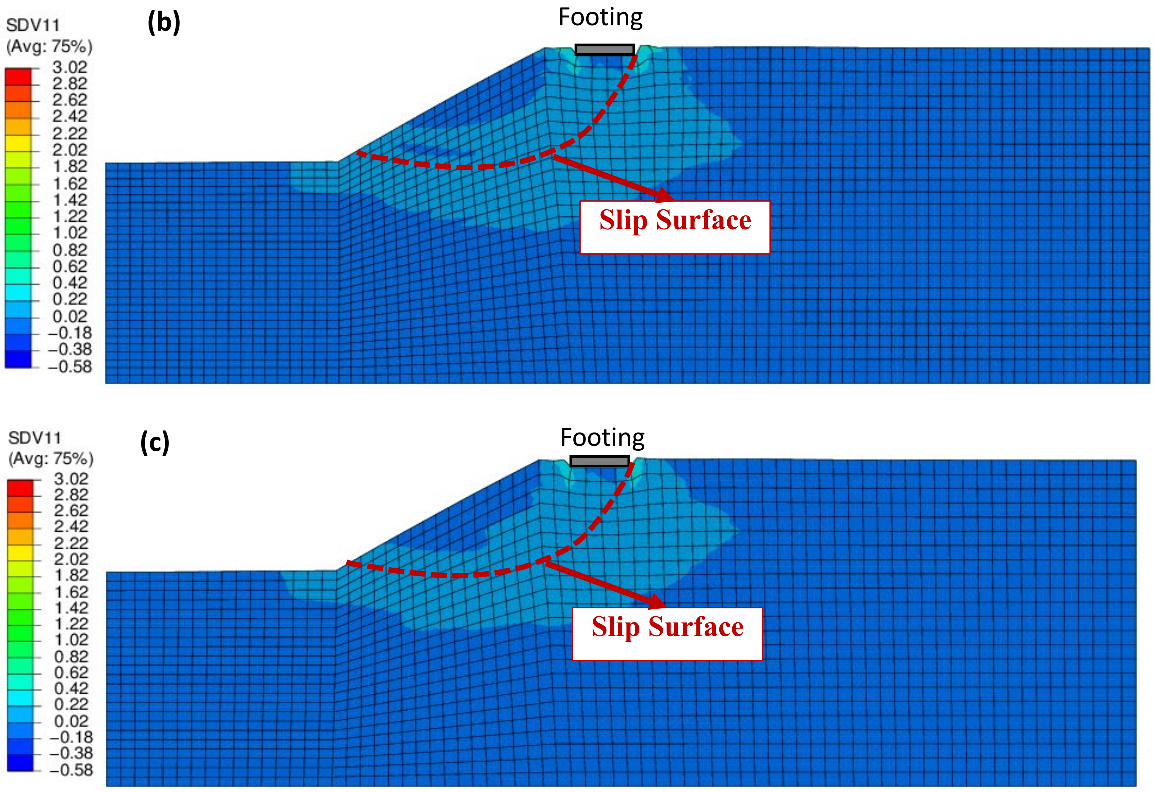

Fig. 22 Shear strain distribution in the soil predicted by the G&S model at at $s/B = 0.12$ with different mesh sizes: (a) 0.20 m; (b) 0.25 m; (c) 0.30 m

6. Response of retaining wall for level sand ground

Fig. 23 shows a soil domain measuring 10 m in length and 4.5 m in depth, with a rigid retaining wall positioned on the right side of the backfill soil. The wall has a height of $h_w = 4\ m$ and is assumed to have an ideally smooth surface that prevents the transmission of shear stresses at the interface with the soil. The retaining wall can undergo passive and active horizontal translation, with passive movement towards the backfill and active movement away from it. The bottom, left-side, and right-side boundaries are fully fixed. In all simulations, the bedding plane orientation is horizontal ($\alpha = 0^{\circ}$) and the gravity is applied to the backfill soil while the top surface of the backfill soil is subjected to a uniformly distributed surcharge of 1 kPa. The same soil conditions as in Fig. 16 are used. $l_c = 0.8\ m$ is applied for all simulations. The lateral earth pressure is expressed as σ_h and the wall displacement u is normalised by the height of the wall h_w.

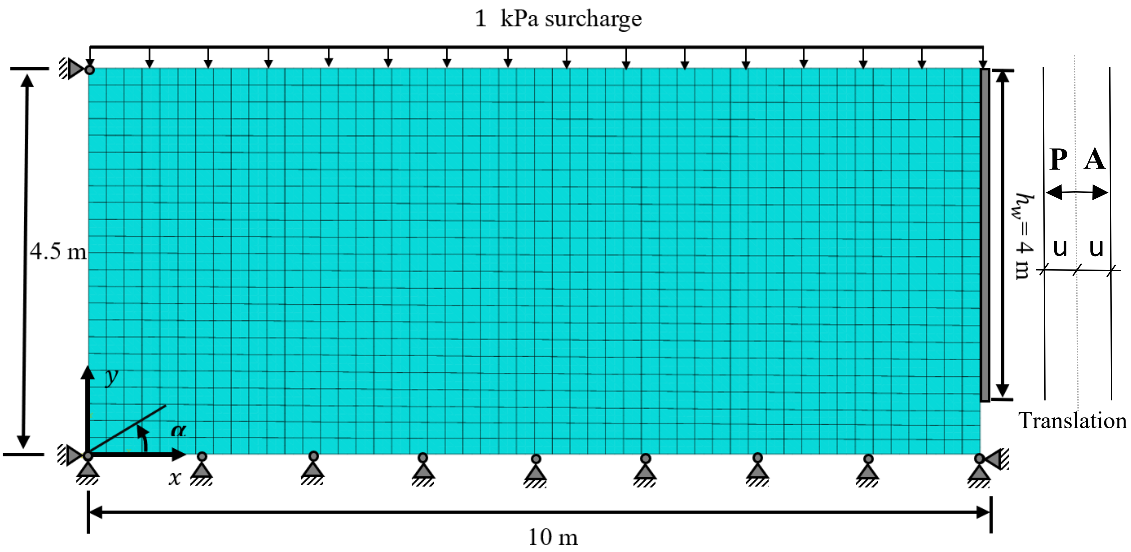

Fig. 23 The boundary conditions of the retaining wall problem

Fig. 24 shows the evolution of σ_h for the active condition. The local model gives mesh-dependent $\sigma_h - u/h_w$ curves. The G&S and ON functions are more efficient than GD function in reducing the mesh-dependency. σ_h reaches the smallest value at $u/h_w \approx 0.015$ and then increases with u/h_w. This is caused by the strain softening of sand. Similar results have been reported in Nübel and Huang (2004), Widulinski et al. (2011) and Guo and Zhao (2015). For the passive condition, the nonlocal models give similar results (Fig. 25).

Fig. 26 shows the strain localization pattern predicted by local model. The shear band orientation in the backfill is directly measured from shear strain contours at $u/h_w = 5\%$ (Fig. 27). The angle of the shear band under active earth condition is larger than that under passive one. The angle of the shear band under active earth pressure decreases with increasing mesh size, while that under passive earth pressure increases. For both cases, the angle range of the local model ($62^{\circ} - 66^{\circ}$) is larger than that of the nonlocal models ($31^{\circ} - 36^{\circ}$). The nonlocal functions reduce the range of measured angle which means they reduce mesh dependency, especially for the G&S function, which is almost constant under active earth pressure. Moreover, under passive earth pressure, the angle measured from the G&S function is slightly larger than that of the GD and ON function.

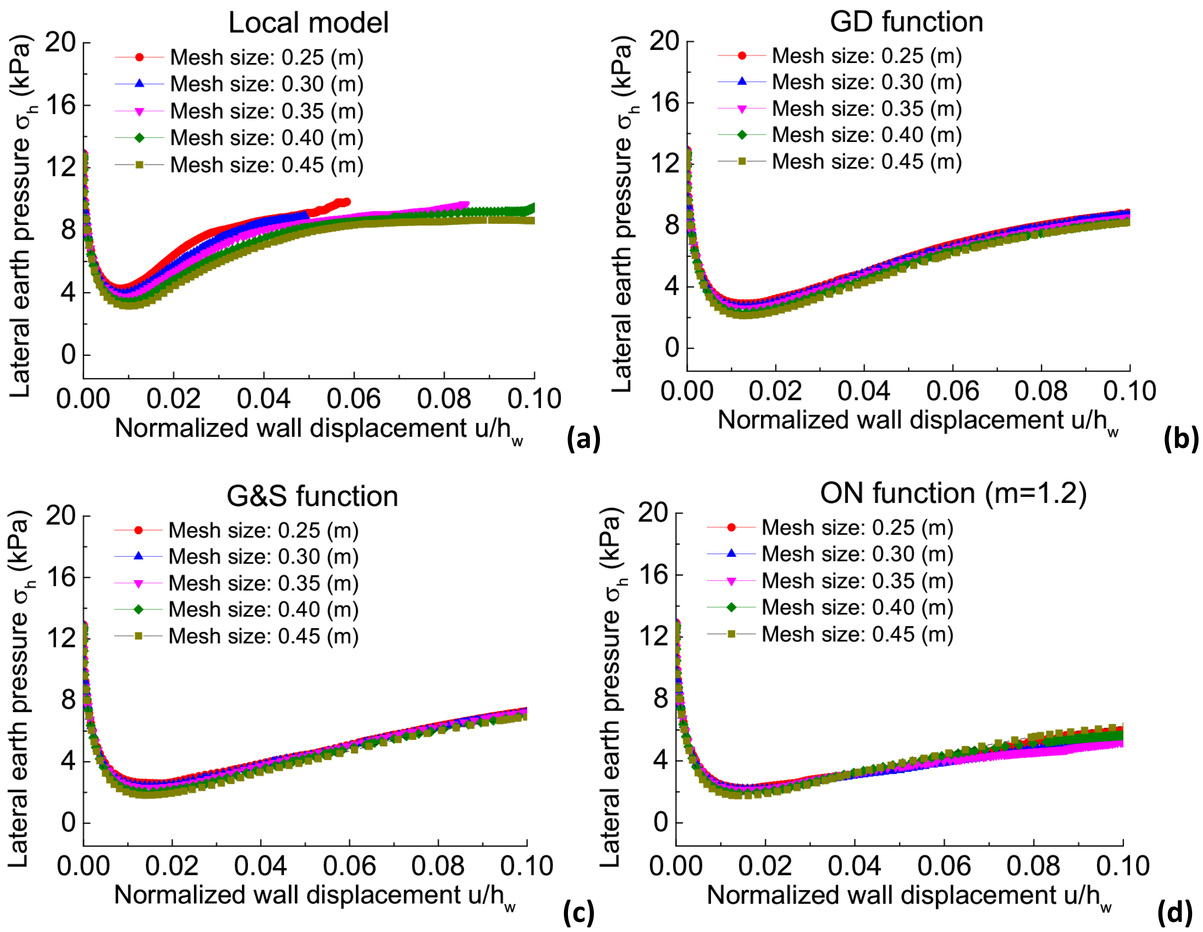

Fig. 24 The comparison of the retaining wall response on the sand under active failure condition: (a) Local model; (b) GD function; (c) G&S function; (d) ON function

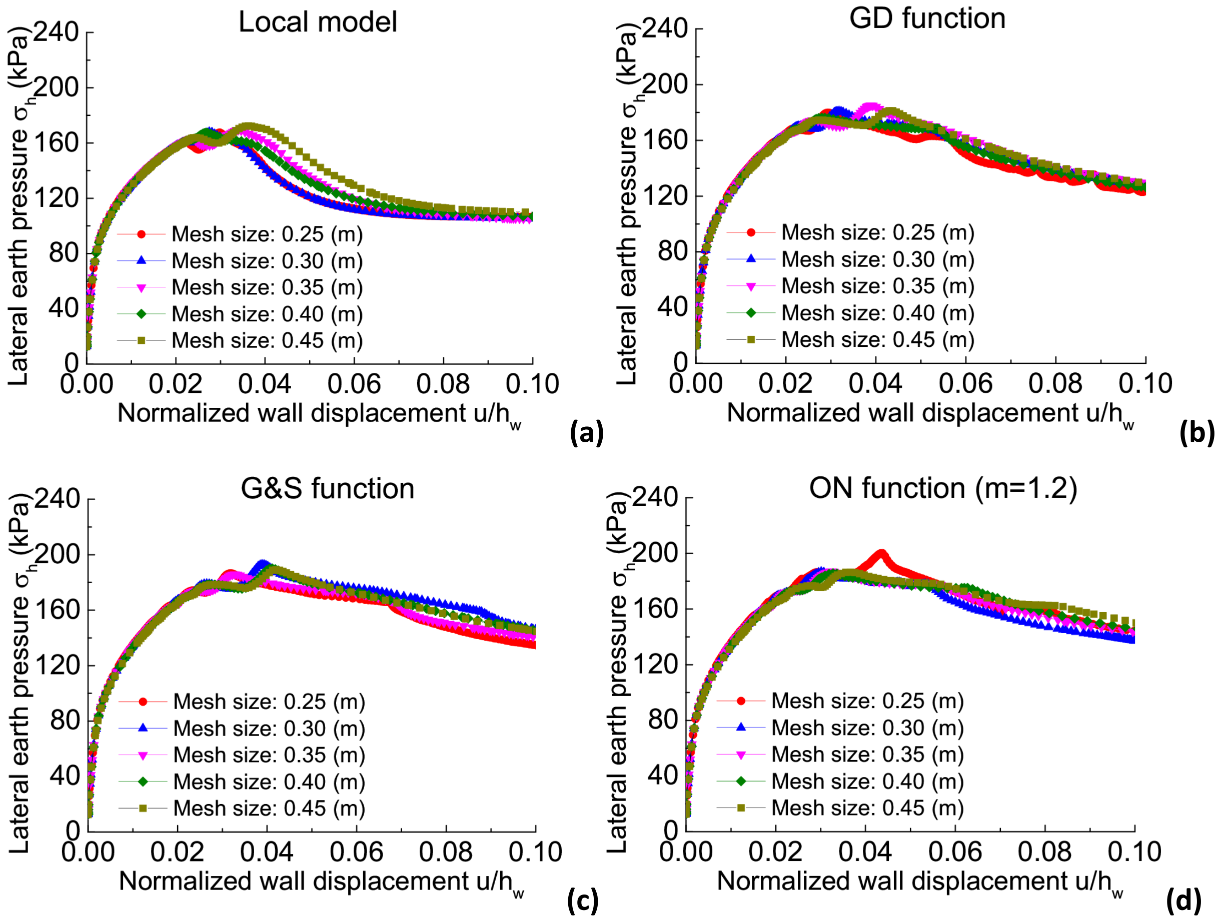

Fig. 25 Comparison of the retaining wall response on the sand under passive failure condition: (a) Local model; (b) GD function; (c) G&S function; (d) ON function

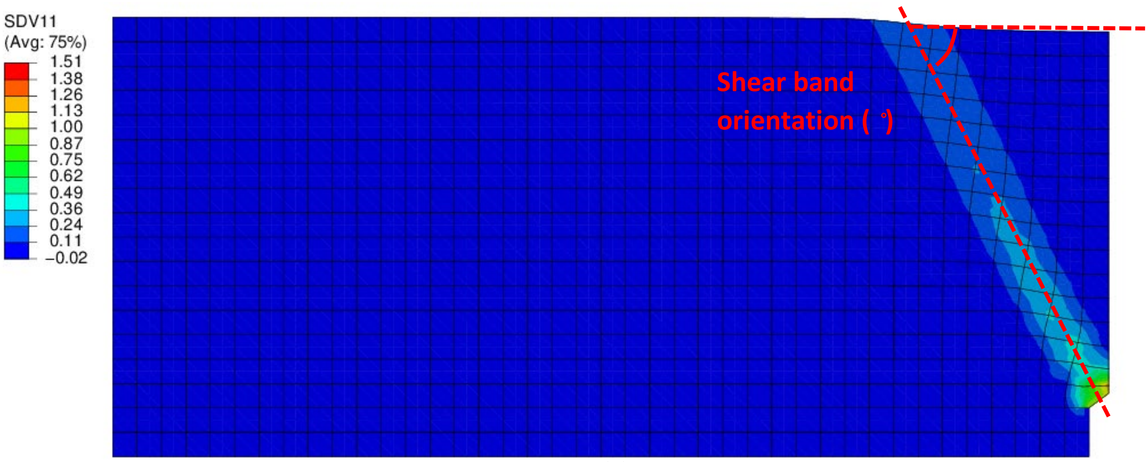

(a)

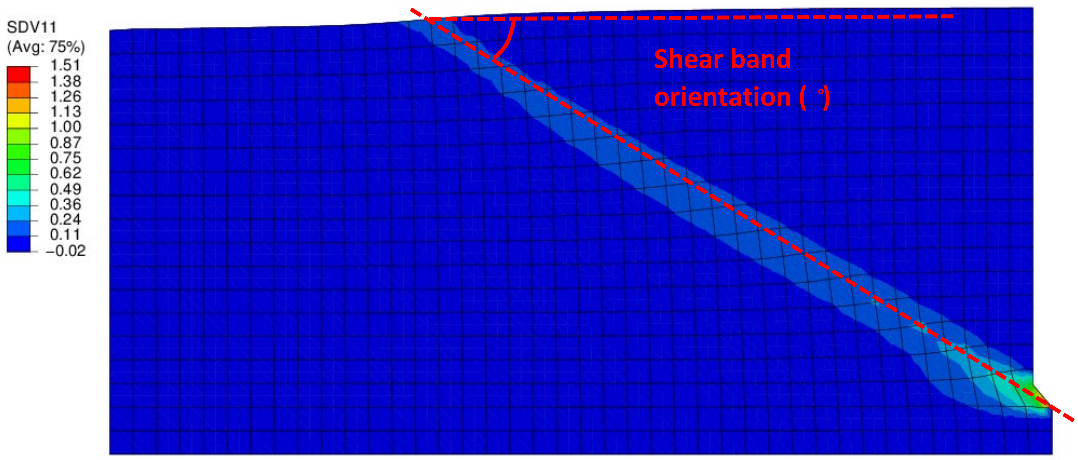

(b)

Fig. 26 Shear band predicted by the G&S model after the retaining wall at $u/h_w = 0.05$: (a) active condition and (b) passive condition

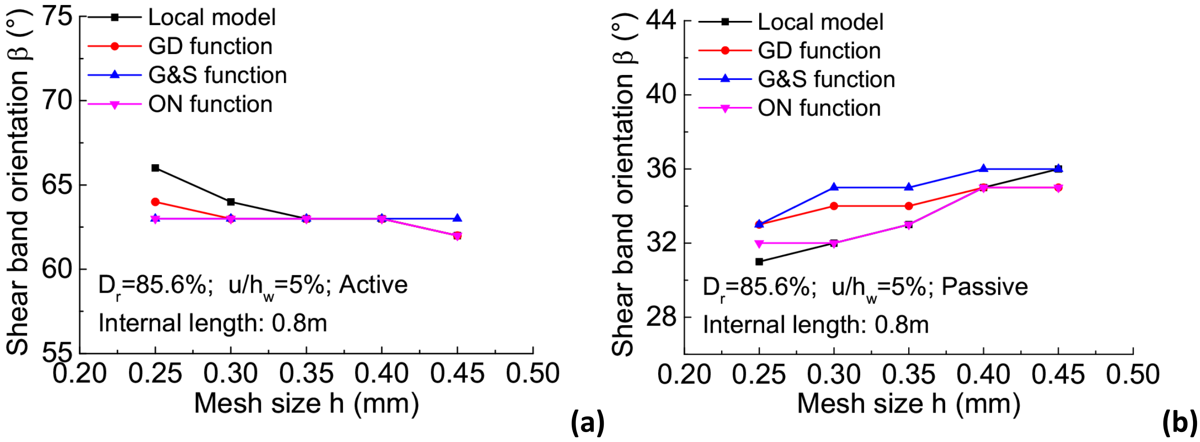

Fig. 27 Comparison of shear band orientation for retaining wall: (a) active failure condition (b) passive failure condition

7. Conclusion

The performance of three different weight functions for nonlocal regularisation have been evaluated, including the GD, G&S and ON functions. An anisotropic sand model accounting for evolution of anisotropy is used. The increment of void ratio is assumed nonlocal, which has a significant influence on strain softening. Different BVPs have been simulated, including drained and undrained plane strain compression, response of strip footings (level ground and slope) and a retaining wall (passive and active conditions). The main conclusions are:

(a) All the nonlocal methods are effective in reducing the mesh dependency of the force-displacement relationship in plane strain compression. The GD method gives less satisfactory results because the local value is contributing most to the nonlocal variable. The nonlocal regularization can reduce the mesh dependency of shear band thickness when the mesh size is smaller than the internal length. It is difficult to get mesh-independent shear band orientation in either drained or undrained condition. This could be due to that only the void ratio increment is assumed nonlocal. More mesh independent results could be obtained if more state variables that affect strain softening are assumed nonlocal.

(b) Nonlocal regularization can effectively reduce the mesh dependency of the force-displacement curves for strip footings. The ON method gives excessive overprediction of volume expansion for soil elements around the footings on a level ground, leading to an unrealistically steep reduction of the reaction force after peak.

(c) All three nonlocal functions give mesh-independent results for the active and passive earth pressures on the retaining wall. The shear band orientation predicted by the three functions shows small variation with the mesh size.

The G&S method is thus a better option for nonlocal regularisation of sand models. It does not require extra parameters and assumes that the local variable does not contribute to the nonlocal one. The GD function gives more mesh dependent results than the G&S function. The extra parameter m for the ON method can be determined using plane strain compression and used for the other BVPs. But the assumption that the local variable can make negative contribution to the nonlocal one may not be realistic. For instance, this assumption can cause very steep reduction of the reaction force on a strip footing on level sand ground.

Data Availability Statement

All code, models, and data generated or used of this study are available from the corresponding author upon reasonable request.

Acknowledgements

The support of the International Exchanges grants of the Royal Society (IES\R1\201132; IEC\NSFC\223020) is acknowledged.

References

Aifantis, E. C. 1984. "Microscopic processes and macroscopic response." *Mechanics of engineering materials*, C. S. Desai and R. H. Gallagher, eds., Wiley, New York, 1–22.

Alsaleh, M., Voyiadjis, G. and Alshibli, K. 2006. "Modelling strain localization in granular materials using micropolar theory: mathematical formulations." *Int. J. Numer. Anal. Methods Geomech*. 30(15): pp.1501-1524.

Alshibli, K.A., Alsaleh, M.I. and Voyiadjis, G.Z. 2006. "Modelling strain localization in granular materials using micropolar theory: Numerical implementation and verification." *Int. J. Numer. Anal. Methods Geomech*. 30: pp. 1525–1544.

Bažant, Z. P. and Gambarova, B. 1984. "Shear crack in concrete: Crack band microplane model." *J. Struct. Eng*., 110(9): 2015–2035.

Bazant, Z.P. and Jirasek, M. 2002. "Nonlocal integral formulations of plasticity and damage: Survey of progress." *J. Eng. Mech.* 128(11): 1119–1149.

Cui, W., Wu, X., Potts, D.M. and Zdravković, L. 2023. "Nonlocal strain regularisation for critical state models with volumetric hardening." *Comput. Geotech.* 157: pp. 105350.

de Borst, R. and Mühlhaus, H.B. 1992. "Gradient-dependent plasticity: Formulation and algorithmic aspects." *Int. J. Numer. Methods Eng.* 35(3): pp. 521–539.

de Borst, R., Sluys, L.J., Muhlhaus, H.B. and Pamin, J. 1993. "Fundamental issues in finite element analyses of localization of deformation." *Eng. Comput.* 10(2): pp. 99–121.

Dorgan, R.J. and Voyiadjis, G.Z. 2003. "Nonlocal dislocation based plasticity incorporating gradients of hardening." *Mech. Mater.* 35(8): pp. 721–732.

Eringen, A.C. 1972. "Nonlocal polar elastic continua." *Int. J. Eng. Sci*. 10(1): 1–16.

Eringen, A.C. and Kim, B.S. 1974. "Stress concentration at the tip of a crack." *Mech. Res. Commun*. 1: 233–237.

Galavi, V. and Schweiger, H. 2010. "Nonlocal Multilaminate Model for Strain Softening Analysis." *Int. J. Geomech.* 10(1): pp.30-44.

Gao, Z.W. and Zhao, J.D. 2013. "Strain localization and fabric evolution in sand." *Int. J. Solid Struct*. 50: pp.3634-3648.

Gao, Z.W., Li, X. and Lu, D.C. 2022. "Nonlocal Regularization of an Anisotropic Critical State Model for Sand." *Acta Geotech.* 17(2): pp. 427–439.

Gao, Z.W., Lu, D.C. and Du, X. 2020. “Bearing Capacity and Failure Mechanism of Strip Footings on Anisotropic Sand.” *J. Eng. Mech*. 146(8): pp.04020081.

Gao, Z.W., Zhao, J.D. and Li, X. 2021. “The deformation and failure of strip footings on anisotropic cohesionless sloping grounds.” *Int. J. Numer. Anal. Methods Geomech*. 45(10): pp. 1526–1545.

Gao, Z.W., Zhao, J.D., Li, X.S. and Dafalias, Y.F. 2014. “A critical state sand plasticity model accounting for fabric evolution.” *Int. J. Numer. Anal. Meth. Geomech*. 38(4): pp.370-390.

Guo, N. and Zhao, J. 2015. “Multiscale insights into classical geomechanics problems.” *Int. J. Numer. Anal. Methods Geomech*. 40(3): pp. 367–390.

Guo, P. and Stolle, D. 2013. “Coupled analysis of bifurcation and shear band in saturated soils.” *Soils Found.* 53(4): 525–539.

Higo, Y. 2004. “*Instability and Strain Localization Analysis of Water-Saturated Clay by Elasto-Viscoplastic Constitutive Models.*” Ph.D. thesis, Kyoto University, Kyoto.

Kimura, T., Kusakabe, O. and Saitoh, K. 1985. “Geotechnical model tests of bearing capacity problems in a centrifuge.” *Geotechnique* 35(1): pp.33–45.

Lazari, M., Sanavia, L. and Schrefler, B.A. 2015. “Local and non-local elasto-viscoplasticity in strain localization analysis of multiphase geomaterials.” *Int. J. Numer. Anal. Methods Geomech.* 39(14): pp. 1570–1592.

Li, X.S. and Dafalias, Y.F. 2012. “Anisotropic Critical State Theory: Role of Fabric.” *J. Eng. Mech*. 138(3): pp.263-275.

Lu, D.C., Liang J.Y., Du, X.L., Ma, C. and Gao, Z.W. 2019. “Fractional elastoplastic constitutive model for soils based on a novel 3D fractional plastic flow rule.” *Comput. Geotech.* 105: pp. 277-290.

Lu, D.C., Zhang, Y.N., Zhou, X., Su, C.C., Gao, Z.W. and Du, X.L. 2023. “A robust stress update algorithm for elastoplastic models without analytical derivation of the consistent tangent operator and loading/unloading estimation.” *Int. J. Numer. Anal. Methods Geomech.* 47: pp. 1022-1050.

Lu, D.C., Zhou, X., Wang, G.S. and Du, X.L. 2019. “A 3D fractional elastoplastic constitutive model for concrete material.” *Int. J. Solids Struct.* 165: pp. 160-175.

Lü, X., Bardet, J.-P. and Huang, M. 2009. “Numerical solutions of strain localization with nonlocal softening plasticity.” *Comput. Methods Appl. Mech. Eng.* 198(47-48): pp. 3702–3711.

Mallikarachchi, H. 2019. "*Constitutive modelling of shear localisation in saturated dilative sand*." Ph.D. thesis, University of Cambridge, Cambridge.

Mallikarachchi, H. and Soga, K. 2020. "A two-scale constitutive framework for modelling localised deformation in saturated dilative hardening material." *Int. J. Numer. Anal. Methods Geomech.* 44(14): pp.1958-1982.

Mühlhaus, H.B. 1986. "Scherfugenanalyse bei Granularem material im rahmen der cosserat-theorie." *Ingenieur-Archiv* 56(5): pp. 389–399.

Nübel, K. and Huang, W. 2004. "A study of localized deformation pattern in granular media." *Comput. Methods Appl. Mech. Eng.* 193(27–29): pp. 2719–2743.

Oka, F., Adachi, T. and Yashima A. 1995. "A strain localization analysis using a viscoplastic softening model for clay." *Int. J. Plast.* 11(5): 523–45.

Okochi, Y. and Tatsuoka, F. 1984. "Some factors affecting K0-values of sand measured in triaxial cell." *Soils Found*. 24(3): pp.52–68.

Singh, V., Stanier, S., Bienen, B. and Randolph, M. 2021. "Modelling the behaviour of sensitive clays experiencing large deformations using non-local regularisation techniques." *Comput. Geotech.* 133: p. 104025.

Summersgill, F., Kontoe, S., and Potts, D. 2017. "On the use of nonlocal regularisation in slope stability problems." *Comput. Geotech.* 82: pp.187–200.

Tang, H., Hu, Z. and Li, X. 2013. "Three-dimensional pressure-dependent elastoplastic Cosserat continuum model and finite element simulation of strain localization." *Int. J. Appl. Mech.* 05(03): pp. 1350030.

Vermeer, P.A. and Brinkgreve, R.B.J. 1994. "*A new effective non-local strain measure for softening plasticity*."R. Chambon, J. Desrues, I. Vardoulakis (Eds.), Localization and Bifurcation Theory for Soil and Rocks, Balkema, Rotterdam, pp. 89-100.

Wang, W., Sluys, L. and De Borst, R. 1997. "Viscoplasticity for instabilities due to strain softening and strain-rate softening." *Int. J. Numer. Methods Eng.* 40(20): pp.3839–3864.

Widulinski, Ł., Tejchman, J., Kozicki, J. and Lesniewska, D. 2011. "Discrete simulations of shear zone patterning in sand in earth pressure problems of a retaining wall." *Int. J. Solids Struct.* 48: pp. 1191–1209.

Xue, D., Lü, X., Huang, M. and Lim, K. 2022. "Nonlocal regularized numerical analyses for passive failure of tunnel head in strain-softening soils." *Comput. Geotech.* 148: pp.104834.

Yin, Z.Y., Chang, C.S., Karstunen, M. and Hicher, P.Y. 2010. “An anisotropic elastic–viscoplastic model for soft clays.” *Int. J. Solids Struct.* 47(5): pp.665–677.

Zhao, J.D., Sheng, D.C., Rouainia, M. and Sloan, S.W. 2005. “Explicit stress integration of complex soil models.” *Int. J. Numer. Anal. Methods Geomech*. 29: pp.1209-1229.

Zhou, X., Lu, D.C., Su, C.C., Gao, Z.W., Du, X.L. 2022. “An unconstrained stress updating algorithm with the line search method for elastoplastic soil models.” *Comput. Geotech.* 143: pp. 104592.

Zhou, X., Lu, D.C., Zhang, Y.N., Du, X.L. and Rabczuk, T. 2021. “An open-source unconstrained stress updating algorithm for the modified Cam-clay model.” *Comput. Methods Appl. Mech. Eng.* 390: pp. 114356.